

Low bit-flip rate probabilistic error cancellation

Mathys Rennela* and Harold Ollivier†
DIENS Ecole Normale Supérieure,
45 rue d'Ulm, 75005 Paris
PSL University, CNRS, INRIA

Noise remains one of the most significant challenges in the development of reliable and scalable quantum processors. While quantum error correction and mitigation techniques offer potential solutions, they are often limited by the substantial hardware overhead required. To address this, tailored approaches that exploit specific hardware characteristics have emerged. In quantum computing architectures utilizing cat-qubits, the inherent exponential suppression of bit-flip errors can significantly reduce the qubit count needed for effective error correction. In this work, we explore how the unique noise bias of cat-qubits can be harnessed to enhance error mitigation efficiency. Specifically, we demonstrate that the sampling cost associated with probabilistic error cancellation (PEC) methods can be substantially lowered when applied to circuits built on cat-qubits, provided the gates used preserve the noise bias. Our error mitigation scheme is benchmarked across various quantum machine learning circuits, showcasing its practical advantages.

I. INTRODUCTION

a. Context. Quantum error correction techniques aim to revert the computational errors which unavoidably arise during the execution of quantum circuits. However, the physical qubit count overhead they impose make them impractical for smaller machines.

Quantum error mitigation restricts the task of handling errors to improving the accuracy of the expectation values obtained by sampling the output from quantum circuits. In doing so, the cost of handling errors shifts from a space overhead (the qubit count required to correct errors) to a time overhead (the number of times one needs to run quantum circuits to mitigate errors). In essence, error mitigation aims to minimize the space overhead in an attempt to make the smallest possible quantum devices deliver useful computational power.

In this context, Probabilistic Error Cancellation (PEC) is an error mitigation technique that relies on the possibility to approximate the expectation value of an observable measured on a quantum state prepared by a noiseless circuit as the average value of measurement results taken over a quasi-probabilistic distribution of noisy quantum circuits (see [31] for the original techniques and, e.g. [10, 12, 29, 30] for improvements and guarantees). This allows to replace the execution of a noiseless circuit with that of noisy but easily implementable ones, while yielding an unbiased estimator for the expectation value of observables on the noiseless circuits.

This method has been put to work for numerous use cases, for example for superconducting quantum architecture with crosstalk [33], or in the mitigation of Markovian noise [11], or in a setting in which one learns the noise associated to a given system [28].

Thanks to its appealing feature of being hardware and

algorithm agnostic, PEC is easy to use. Yet, this also means that PEC does not exploit knowledge of error propagation within the quantum circuits of interest in order to perform more efficient simulations. One might thus ask, following [6, Open Question 3], whether PEC can be further optimized if one is willing to specialize it to a given hardware or algorithm.

In this paper, we provide a positive answer to the previous open question. We do so by considering cat-qubit architectures [16]. Using a biased noise error model, and with the knowledge of the propagation of errors within bias-preserving circuits, we introduce a variant of PEC that outperforms standard PEC in terms of sampling cost overhead for achieving a given target variance for the expectation value of an observable measured at the output of the noiseless circuit. We derive general theoretical performance guarantees, provide numerical explorations of our method and describe their impact for specific machine learning applications.

b. Overview of results. PEC operates by sampling noisy circuits to construct an approximation of an ideal noiseless circuit given as input. When such ideal circuit is provided as a sequence of layered gates, PEC constructs a collection of noisy circuits from each layer by independently adding extra gates that mitigate the effect of the noise on average. This unfortunately results in a quantum sampling cost that increases exponentially with the number of layers.

To improve over such a situation, we seek to reduce the base and exponent of the exponential quantum sampling cost that PEC incur. We do so by grouping the added gates together by commuting them through the various noisy layers of the circuit. They are then combined into a single additional layer. This is effectively performing PEC through block sampling. We thus refer to this method as *Block-PEC*. We then derive theoretical guarantees to obtain performance improvements. It shows that Block-PEC trades part of the quantum sampling cost for a classical pre-processing step which calculates quasi-probabilities. This results in a quantum sam-

*Electronic address: mathys.rennela@ens.fr

†Electronic address: harold.ollivier@ens.fr

pling exponential in the qubit count of the circuit rather than exponential in the qubit count *and* the circuit depth as is the case for conventional PEC approach.

We then show that cat-qubit architectures — architectures for which bit-flips are exponentially suppressed with a parameter that can be tuned experimentally [16] — via their 1 and 2-qubit bias-preserving gates, mapping phase flips to phase flips, naturally satisfy the conditions required for efficient Block-PEC. It thus provides the first quantum error mitigation technique which specifically targets such architectures. We then relax the requirements of Block-PEC by considering circuits which are bias-preserving on a given subspace of the full Hilbert space accessible to the computer.

Finally, we explore the practical performance of this technique through numerical simulations using small size circuits corresponding to a variety of bias-preserving circuits at the core of machine learning algorithms and computational finance applications of quantum computing. This is done using various biased noise model assumptions (i.e. with and without correlated errors for 2-qubit gates). We find a clear improvement for parameterized quantum circuits formed by matchgates, and in particular Reconfigurable Beam Splitter (RBS) gates, which are widely used in quantum machine learning algorithms for NISQ computers, see e.g. [7, 8, 15, 17, 25].

c. Related work. PEC is a well established error mitigation technique available in various open source packages (see e.g. [22]). From [29], we know that standard PEC is optimal (in terms of sampling cost) when applied on one n -qubit layer subjected to dephasing noise. Moreover, it has been established that using a continuous set of ideal gates, containing all Z -axis rotations for arbitrary angles, would not help lower the cost of PEC, as explained in [29, Sec. 5].

Previous works have nonetheless provided improvements to PEC by optimizing the sampling cost taking into account the gates within the past light-cone of a given observable, as only those contribute to the errors affecting the measured expectation value [32].

d. Outline. After an overview of the mathematical formalism of probabilistic error cancellation (Section II), we introduce Block-PEC, and we outline the conditions under which it can be implemented (Section III). We then provide performance guarantees for Block-PEC (Section IV), followed by a numerical analysis of the implementation of Block-PEC on concrete applications (Section V). We conclude in Section VI, focusing on the prospects of this approach, and placing it in the context of hardware-specific error mitigation techniques.

II. PRELIMINARIES

A. Quantum channels

Quantum channels are completely positive trace preserving operators acting on density matrices. They will

be written using sans-serif fonts such as \mathbb{C} . A unitary channel associated to a unitary operator U is defined as $\mathbb{U}(\cdot) = U \cdot U^\dagger$. By convenience, we will often refer to \mathbb{U} as a unitary operator.

While noise channels can in principle correspond to any CPTP maps, we restrict our study to convex combinations of unitary channels $\mathbb{N} = \sum_{\mathbb{V} \in \mathbb{V}} \alpha(\mathbb{V})\mathbb{V}$ with $\alpha(\mathbb{V}) \geq 0$, $\sum_{\mathbb{V}} \alpha(\mathbb{V}) = 1$, and where \mathbb{V} is a set of unitary channels (e.g. Pauli channels where the unitary belongs to the Pauli group).

Definition II.1 (Noisy unitary channel). *The noisy version of a unitary channel \mathbb{U} under the action of the noise channel \mathbb{N} is written*

$$\tilde{\mathbb{U}} = \mathbb{N} \circ \mathbb{U} = \sum_{\mathbb{V} \in \mathbb{V}} \alpha(\mathbb{V})\mathbb{V} \circ \mathbb{U}. \quad (1)$$

A layered circuit is a circuit which can be defined as a succession of unitaries $U = U_d \dots U_1$ so that d is the depth of the circuit, where U_l is the unitary corresponding to the l -th layer of the circuit. With our notation, \mathbb{U}_l is the channel for the l -th layer, so that the full circuit is a unitary channel $\mathbb{U} = \mathbb{U}_d \circ \dots \circ \mathbb{U}_1$. The noisy variant of the quantum channel \mathbb{U} is given by

$$\tilde{\mathbb{U}} = \sum_{\mathbb{V} \in \mathbb{V}_1 \times \dots \times \mathbb{V}_d} \alpha(\mathbb{V})\mathbb{V}_d \circ \mathbb{U}_d \circ \dots \circ \mathbb{V}_1 \circ \mathbb{U}_1, \quad (2)$$

where $\alpha(\mathbb{V}) = \prod_{l=1}^d \alpha_l(\mathbb{V}_l)$ for $\mathbb{V} = (\mathbb{V}_1, \dots, \mathbb{V}_d)$, and each \mathbb{V}_l defined as the generating set of unitaries associated to the noise channel $\mathbb{N}_l = \sum_{\mathbb{V}_l \in \mathbb{V}_l} \alpha_l(\mathbb{V}_l)\mathbb{V}_l$.

B. cat-qubits and dephasing noise

cat-qubits are superconducting qubits which can be physically implemented in such a way that bit flip errors are exponentially suppressed, at the cost of a linear increase of the phase flip error rate (see [16] for a detailed presentation of cat-qubits). In other words, cat-qubits are associated with a biased noise model, heavily biased towards phase flip errors.

There is experimental evidence that phase flips errors are drastically rarer than bit flip errors (10^8 times rarer in the experiments in [5], for example). In the present work, we choose to ignore bit flips altogether (we further explain this choice in Appendix B). To make our results more concrete, we make use of two simplified dephasing noise models. The first one inserts correlated phase flips after each gate on the qubits it has been acting upon. More precisely, we chose to consider that after a gate acting on the set of n qubits A , the following channel acts upon these qubits:

$$\mathbb{C}_p^{[A]} = (1-p)\mathbb{I}^{\otimes n} + \sum_{I^{\otimes n} \neq B \subseteq A} \frac{1}{2^n - 1} p Z_{[B]}, \quad (3)$$

where p is the 1-qubit phase flip error probability, and $Z_{[B]}$ is the Pauli unitary operator defined for any set $B \subseteq A$ of qubits by

$$Z_{[B]} = \left(\bigotimes_{i \in B} Z_i \right) \otimes \left(\bigotimes_{i \in A \setminus B} I_i \right), \quad (4)$$

so that $Z_\emptyset = I^{\otimes n}$. Such correlations have been observed in cat-qubit architectures for 1 and 2-qubit gates (see e.g. [16]). The second model is a more drastic approximation but yields simpler analytic calculations. It consists of applying single qubit dephasing channels on all the qubits a gate is acting upon. In effect, for a gate acting on the set of qubits A , the channel applied after the gate is

$$\mathbb{F}_p^{[A]} = \sum_{B \subseteq A: |B|=m} (1-p)^{n-m} p^m Z_{[B]}. \quad (5)$$

In practice, this latter model neglects correlations between the errors within the set of qubits affected by the gate. In Appendix E, we justify that Block-PEC retains its performance when error correlations are taken into account.

C. Overview of Probabilistic Error Cancellation

To compensate the effect of noise, error mitigation techniques such as PEC intend to apply the inverse of the noise channel to the affected quantum systems. While it is not a physically realizable operation (when the noise channel is not unitary), it is nonetheless well defined mathematically.

Indeed (see [10, 31] and also Appendix A), for large classes of noise models, one can rewrite the channel \mathbb{U} corresponding to a noiseless d -layered circuit as a quasi-probabilistic distribution of noisy circuits [10, 31]:

$$\mathbb{U} = \sum_{\mathbb{V} \in \mathbb{V}} \alpha(\mathbb{V}) \mathbb{N}_d \circ \mathbb{V}_d \circ \mathbb{U}_d \circ \dots \circ \mathbb{N}_1 \circ \mathbb{V}_1 \circ \mathbb{U}_1, \quad (6)$$

where $\alpha(\mathbb{V}) = \alpha_1(\mathbb{V}_1) \dots \alpha_d(\mathbb{V}_d)$ for $\mathbb{V} = (\mathbb{V}_1, \dots, \mathbb{V}_d) \in \mathbb{V}$ where the $\alpha_l(\mathbb{V}_l)$'s are given by the resolution of the system of equations defined for each layer by

$$I^{\otimes n_l} = \sum_{\mathbb{V}_l \in \mathbb{V}_l} \alpha_l(\mathbb{V}_l) \mathbb{N}_l \circ \mathbb{V}_l, \quad (7)$$

where $\sum_{\mathbb{V}_l} \alpha_l(\mathbb{V}_l) = 1$, and n_l is the number of qubits that the l -th layer \mathbb{U}_l acts non-trivially on.

Under the assumption that the noisy unitary channels $\tilde{\mathbb{B}}_l = \mathbb{N}_l \circ \mathbb{V}_l \circ \mathbb{U}_l$ correspond to physically implementable gates, PEC determines the expectation value of the noiseless circuit U by randomly sampling a noisy gate $\tilde{\mathbb{B}}_l$ for each layer, and executing the circuit corresponding to $\tilde{\mathbb{B}}_d \dots \tilde{\mathbb{B}}_1$.

The noiseless expectation value $\langle O \rangle_{\text{ideal}} = \text{Tr}[OU(\rho_0)]$ for some observable O (without loss of generality, $\|O\|_\infty = 1$), and given the initial state $\rho_0 = |0\rangle\langle 0|^{\otimes n}$ is such that

$$\langle O \rangle_{\text{ideal}} = \sum_{\mathbb{V}_1, \dots, \mathbb{V}_d \in \mathbb{V}} \alpha_{\mathbb{V}_1} \dots \alpha_{\mathbb{V}_d} \dots \langle O \rangle_{\mathbb{V}_1, \dots, \mathbb{V}_d}. \quad (8)$$

where

$$\langle O \rangle_{\mathbb{V}_1, \dots, \mathbb{V}_d} = \text{Tr}\left[O\tilde{\mathbb{B}}_d \dots \tilde{\mathbb{B}}_1(\rho_0)\right]. \quad (9)$$

Hoeffding's inequality states that the number of samples S required to attain precision δ with PEC, with probability at least $1 - \varepsilon$, is $S \geq \frac{\gamma_{\text{total}}^2}{2\delta^2} \ln\left(\frac{2}{\varepsilon}\right)$, where $\gamma_{\text{total}} = \gamma_d \dots \gamma_1$. In this context, the sampling cost γ_{total} entirely determines the performance of PEC as an error mitigation technique.

In a conventional use of PEC, the sampling cost γ_{total} is in $O(\gamma^{nd})$, where n is the qubit count, d is the circuit depth, and $\gamma \simeq 1 + kp + O(p^2)$ for some constant k determined by the noise model (for dephasing noise, $k = 2$), with 1-qubit error rate p . This makes PEC a reasonable mitigation strategy in the presence of weak gate noise [29].

D. Inverting Pauli noise

As outlined in the previous section, the key requirement for PEC is the ability to write perfect gates as a quasi-probabilistic combination of noisy ones. Whenever the noise channel applied after each ideal gates is a convex combination of Pauli channels, this can be performed rather straightforwardly by writing the inverse as a Taylor series.

Additionally, and this will be crucial for block-PEC, whenever the above convex combination can be restricted to subgroup of the Pauli group, so does the quasi-probabilistic distribution of the inverse.

Theorem II.2. *The inverse of a Pauli-noise channel $\mathbb{N} = (1-p)\mathbb{I} + p\mathbb{A}$, where \mathbb{A} is a convex combination over Pauli channels, is a quasi-probabilistic distribution of Pauli channels.*

Furthermore, if the non trivial Pauli-channels in \mathbb{A} correspond to Pauli operators that form a group, so do the non trivial terms in the quasi-probabilistic distribution of \mathbb{N}^{-1} .

\mathbb{N}^{-1} can be approximated by a channel of the form $(1+p)\mathbb{I} - p\mathbb{A}$.

Proof. Consider a noise channel $\mathbb{N} = (1-p)\mathbb{I} + p\mathbb{A} = (1-p)\mathbb{I} + \sum_{\mathbb{Q} \in \mathbb{Q}} p_{\mathbb{Q}} \mathbb{Q}$, where each \mathbb{Q} is a Pauli channel associated to a probability $p_{\mathbb{Q}}$, so that $\sum_{\mathbb{Q}} p_{\mathbb{Q}} = 1$, and such that \mathbb{Q} is a subgroup of the Pauli group.

Then,

$$N^{-1} = ((1-p)I + pA)^{-1} \quad (10)$$

$$= (1-p) \left(I + \sum_{i>0} \left(-\frac{p}{1-p} A \right)^i \right) \quad (11)$$

$$\approx (1+p)I - pA. \quad (12)$$

The first and second claim of the theorem follow from the group structure of \mathbb{Q} which guarantee that each term in the expansion of $A^i = \left(\sum_{Q \in \mathbb{Q}} p_Q Q \right)^i$ is in \mathbb{Q} .

The third claim (Eq. 12) is obtained by truncating the Taylor series to order 1. \square

III. BLOCK PROBABILISTIC ERROR CANCELLATION

The standard PEC procedure outlined in Section II C is oblivious to the structure of the implementable gate set and noise model save for the actual quasi-probabilistic decomposition of each noisy gate. In this section, we go beyond this generic approach by using a property of the implementable gate set that we call *Pauli-Z compatibility* to modify the Monte Carlo sampling performed in the PEC procedure.

This yields a lower sampling cost — i.e. the number of quantum circuits to run — provided some classical pre-computations can be performed efficiently. We call this improved method *block probabilistic error cancellation* (Block-PEC), as it rearranges the sampling of noisy gates on a per-block basis rather than layer by layer.

After defining Pauli-Z compatibility, we detail how to implement Block-PEC, how to efficiently (classically) compute the coefficients of its quasi-probabilistic distribution, and extend the technique to consider generic gate sets which contain gates which are not Pauli-Z compatible.

A. Pauli-Z compatibility

In order to capture a useful commutation property between implementable gate sets and noise, we define the following property.

Definition III.1 (Pauli-Z compatibility). *Let \mathbb{N} , \mathbb{U} and \mathbb{V} be three sets of unitary operators acting on at most n qubits, where,*

(P1) \mathbb{V} is a group, and a subset of \mathbb{U} ,

(P2) \mathbb{V} is stable by conjugation with elements of \mathbb{U} , i.e.

$$\forall V \in \mathbb{V}, \forall U \in \mathbb{U}, \exists V' \in \mathbb{V}, s.t. U \circ V = V' \circ U; \quad (13)$$

(P3) \mathbb{V} commutes with all \mathbb{N} , i.e.

$$\forall V \in \mathbb{V}, \forall N \in \mathbb{N}, N \circ V = V \circ N. \quad (14)$$

A Pauli-Z string is a n -fold tensor product of single qubit I and Z . Whenever \mathbb{N} is the set of all convex combinations of Pauli-Z strings, we say that (\mathbb{U}, \mathbb{V}) is Pauli-Z compatible.

For convenience, we will say that a gate is Pauli-Z compatible if it is in a set \mathbb{U} such that (\mathbb{U}, \mathbb{V}) is compatible, with \mathbb{V} being the set of all Pauli-Z strings. A circuit is Pauli-Z compatible if it is generated from a Pauli-Z compatible gate set.

In this definition, \mathbb{U} above represents perfect implementable gates for a given architecture. (P1) states that it is possible to single-out a subgroup \mathbb{V} of \mathbb{U} that will be used to apply additional controls after each intended gate. (P2) states that given a sequence of implementable gates, one can apply the additional controls described above at the very end of the circuit.

To make this concrete imagine a 2-gate circuit $U_2 \circ U_1$ with $U_1, U_2 \in \mathbb{U}$, and that one wants to implement instead $V_2 \circ U_2 \circ V_1 \circ U_1$, with $V_1, V_2 \in \mathbb{V}$. Then, using (P2), there exists V'_1 such that $V_2 \circ U_2 \circ V_1 \circ U_1 = V_2 \circ V'_1 \circ U_2 \circ U_1$. Using (P1), $V_2 \circ V'_1$ can be replaced by $V' \in \mathbb{V}$. Finally (P3) guarantees that, in spite of noise operators chosen in \mathbb{N} , the previous pulling of additional controls at the end of the circuit can be performed without modification. For this, let N_1 and N_2 in \mathbb{N} be the noise channels applied after U_1 and U_2 respectively, then (P3) gives $V_2 \circ N_2 \circ U_2 \circ V_1 \circ N_1 \circ U_1 = V' \circ N_2 \circ U_2 \circ N_1 \circ U_1$, with the same V' as in the noiseless case.

With cat-qubit architectures in mind, we can already develop an example of Pauli-Z compatibility. For instance, take $\mathbb{U} = \mathbb{V} \cup \{Z(\theta), ZZ(\theta), \text{CNOT}\}$, where $Z(\theta) = \exp(-i\frac{\theta}{2}Z)$, $ZZ(\theta) = \exp(-i\frac{\theta}{2}Z \otimes Z)$, and \mathbb{V} are all Pauli-Z strings. Then, a straightforward calculation leads to establishing the Pauli-Z compatibility of (\mathbb{U}, \mathbb{V}) .

Moreover, the noise model associated to \mathbb{N} is dephasing, and therefore, the physical intuition behind Pauli-Z compatibility is that any circuit made of gates in \mathbb{U} can be sampled from as a block, by performing all the additional controls of the error cancellation procedure at the end of the circuit, rather than after each gate.

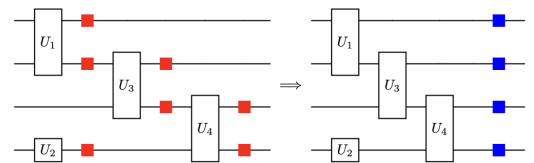


FIG. 1: As shown in the example depicted above, Block-PEC samples from the circuit on the left as a single block of the equivalent circuit on the right, where all of the error locations (in red) have been commuted to the right of the circuit and aggregated (in blue).

B. Block probabilistic error cancellation

Consider a layered circuit $U = U_d \circ \dots \circ U_1$ with layers $U_l \in \mathbb{U}$, each associated to their own noise channel N_l , forming a non-uniform noise model.

Each layer U_l can be decomposed into a quasi-probabilistic distribution of layers obtained by applying a perfect additional control:

$$U_l = \sum_{V_l \in \mathbb{V}} \alpha_{U_l}(V_l) V_l \circ \tilde{U}_l, \quad (15)$$

where $\alpha_{U_l}(V_l)$ are real numbers that depend on the target transformation U_l and the effective noise N_l at layer U_l .

We can now commute all the additional controls V_l to the end of the circuit resulting into a quasi-probabilistic distribution corresponding to U :

$$\begin{aligned} U &= U_d \circ \dots \circ U_1 \\ &= \sum_{V_1, \dots, V_d \in \mathbb{V}} \left[\alpha_{U_d}(V_d) \dots \alpha_{U_1}(V_1) \times \right. \\ &\quad \left. (V'_d \circ \dots \circ V'_1) \circ (\tilde{U}_d \circ \dots \circ \tilde{U}_1) \right] \\ &= \sum_{V \in \mathbb{V}} \alpha_U(V') V' \circ \tilde{U}, \end{aligned} \quad (16)$$

where the last equality uses the group structure of \mathbb{V} , so that V' is associated to a depth-1 circuit formed by the product $\prod_{l=1}^d V'_l$ for V'_l defined as the result of commuting V_l through the noise channels N_k for $k \geq l$ and the gates U_k for $k > l$, and where

$$\alpha_U(V') = \sum_{V_1, \dots, V_d \in \mathbb{V}} \alpha_{U_d}(V_d) \dots \alpha_{U_1}(V_1), \quad (17)$$

for V_1, \dots, V_d such that $V'_d \circ \dots \circ V'_1 = V'$.

Now, we can apply a similar decomposition for $V' = \sum_W \beta_{V'}(W) \tilde{W}$ so that when replaced in Eq. 16, we obtain a new quasi-probabilistic decomposition for U , using only noisy implementable gates:

$$U = \sum_{W \in \mathbb{V}} \delta_U(W) \tilde{W} \circ \tilde{U}, \quad (18)$$

with $\delta_U(W) = \sum_{V' \in \mathbb{V}} \alpha_U(V') \beta_{V'}(W)$.

The interest is that instead of requiring a sample for each layer of the circuit, only a single layer needs to be sampled as long as the new coefficients $\delta_U(W)$ can be efficiently computed classically as to ensure that sampling from this distribution can be done efficiently.

To understand why our per-block approach can reduce the sampling overhead, consider a limiting case where the additional controls V_i as well as V can be applied without introducing additional noise. The standard probabilistic error cancellation gives:

$$U = \sum_{V_1, \dots, V_d \in \mathbb{V}} \alpha_{U_1}(V_1) \dots \alpha_{U_d}(V_d) V_d \circ \tilde{U}_d \circ \dots \circ V_1 \circ \tilde{U}_1, \quad (19)$$

which in turn requires a sampling overhead that scales as the square of

$$\gamma_{\text{std}} := \sum_{V_1, \dots, V_d \in \mathbb{V}} |\alpha_{U_1}(V_1) \dots \alpha_{U_d}(V_d)|, \quad (20)$$

see [31].

For our per-block method this is instead equal to

$$\gamma_{\text{blk}} := \sum_{V' \in \mathbb{V}} \left| \sum_{\substack{V_1, \dots, V_d \in \mathbb{V} \\ V'_d \circ \dots \circ V'_1 = V'}} \alpha_{U_1}(V_1) \dots \alpha_{U_d}(V_d) \right|. \quad (21)$$

The inequality $\gamma_{\text{std}} \geq \gamma_{\text{blk}}$ follows from the triangle inequality.

C. Computing Block-PEC coefficients

Calculating naively the coefficients of Block-PEC as sums of products of coefficients of conventional PEC as presented in Equation 21 can take up to $2^{2n(d-1)}$ operations, for a d -layer circuit with $d \geq 2$.

This classical pre-processing cost can be drastically reduced by calculating Block-PEC coefficients recursively, building up on the calculations of the coefficients in sub-circuits.

Indeed, one can observe that any per-block coefficient can be rewritten as follows:

$$\alpha_U(V') = \sum_{\substack{V_1, \dots, V_d \in \mathbb{V} \\ V'_d \circ \dots \circ V'_1 = V'}} \alpha_{U_1}(V_1) \dots \alpha_{U_d}(V_d) \quad (22)$$

$$\begin{aligned} &= \sum_{V_d \in \mathbb{V}} \alpha_{U_d}(V_d) \times \\ &\quad \sum_{\substack{V_1, \dots, V_{d-1} \in \mathbb{V} \\ V'_d \circ \dots \circ V'_1 = V'}} \alpha_{U_1}(V_1) \dots \alpha_{U_{d-1}}(V_{d-1}) \end{aligned} \quad (23)$$

$$= \sum_{V_d \in \mathbb{V}} \alpha_{U_d}(V_d) \sum_{\substack{W \in \mathbb{V} \\ V'_d \circ W' = V'}} \alpha_{U_{d-1} \circ \dots \circ U_1}(W'), \quad (24)$$

where W' should be thought of as the result of commuting V_1 to V_{d-1} through all gates and noise channels to the end of the circuit until reaching, but not crossing, the d -th layer.

This opens the door to a recursive calculation of per-block coefficients, for the sub-circuit $U_{l+1} U_l \dots U_1$, from the per-block coefficients for the sub-circuit $U_l \dots U_1$.

For any n -qubit $V \in \mathbb{V}$, where \mathbb{V} is the set of Pauli- Z string, calculating $\alpha_{U_2 U_1}(V)$ takes at most $|\mathbb{V}|^2 \leq 2^{2n}$ operations. Similarly, calculating each $\alpha_{U_{l+1} U_l \dots U_1}(V)$ knowing $\{\alpha_{U_l \dots U_1}(V)\}_V$ takes at most $|\mathbb{V}|^2 \leq 2^{2n}$ operations. Starting from 2^n coefficients, one needs to perform 2^n multiplications and additions to compute all the per-block coefficients $\{\alpha_{U_{l+1} U_l \dots U_1}(V)\}_V$.

Algorithm 1 Block-PEC coefficient calculation

```

function COMPUTE-COEFFICIENTS( $U_{l+1} \circ \dots \circ U_1, V'$ )
  if  $l = 1$  then
    return list( $\alpha_{U_2}(V_2)\alpha_{U_1}(V_1)$  for  $V_2, V_1 \in \mathbb{V}^2$ )
  for all  $V_{l+1} \in \mathbb{V}$  do
     $\beta(V_{l+1}) \leftarrow 0$ 
    for all  $W \in \mathbb{V}$  do
      if  $V'_d \circ W = V'$  then
         $\beta(V_{l+1}) \leftarrow \beta(V_{l+1}) + \alpha_{U_d}(V_d) \cdot$ 
         $\text{COMPUTE-COEFFICIENTS}(U_l \circ \dots \circ U_1, W')$ 
    return list( $\beta(V_{l+1})$  for  $V_{l+1} \in \mathbb{V}$ )
  
```

All in all, calculating recursively all per-block coefficients of a d -layered circuit takes at most $(d-1)2^{2n}$ operations, instead of $2^{2n(d-1)}$ for the naive approach.

The effect of Block-PEC can be seen as replacing the relatively easy sampling method of the conventional PEC approach with a more complex sampling which extracts some classically computable quantities, and thereby reduces the number of quantum samples required for a given precision.

D. Hybrid Block-PEC for circuits with generic gates

We have previously established that (\mathbb{U}, \mathbb{V}) is Pauli- Z compatible, where \mathbb{V} is the set of all Pauli- Z string, and $\mathbb{U} = \mathbb{V} \cup \{Z(\theta), ZZ(\theta), \text{CNOT}\}$. Both the T gate ($T = Z(\pi/4)$) and the phase gate ($S = Z(\pi/2)$) are in \mathbb{U} . The Hadamard gate H together with the set \mathbb{U} form a universal gate set, but $(\mathbb{U} \cup \{H\}, \mathbb{V})$ is not Pauli- Z compatible. This is especially problematic considering that the Hadamard gate cannot be replaced by a resource state in universal quantum computing [19].

Nonetheless, our per-block technique can be applied to Pauli- Z compatible sub-circuits. This results in a hybrid Block-PEC / PEC simulation of the noiseless circuit using samples obtained from the noisy quantum computer. The advantage given by the Block-PEC technique remains, as the lower sampling cost of each sub-circuit directly reduces the sampling cost of the full circuit.

In this context, it would be beneficial to implement circuit rewriting rules which optimize quantum circuit layouts for our error mitigation schemes for example, by optimizing the positions of Hadamard gates within the circuit or to move Hadamard gates along the wires of the circuit. We leave this for future research.

IV. PERFORMANCE ANALYSIS OF BLOCK-PEC

Section III derived a sampling cost improvement for block-PEC in the limiting case where additional controls are noiseless. In the following paragraphs, we examine more realistic situations for specific gate sets.

A. Strictly bias-preserving gates

a. Pauli- Z compatibility. A gate is said to be bias-preserving if it does not turn phase-flip errors into bit-flip errors. In other words, phase-flip errors are mapped to phase-flip errors, preserving phase-flip biases (see Appendix C for a complete mathematical characterization).

Definition IV.1. A n -qubit gate is bias-preserving if its unitary matrix representation G is such that for every n -by- n unitary diagonal matrix D , there is a n -by- n unitary diagonal matrix D' such that $GD = D'G$.

Examples of bias-preserving gates are the gates X , Z , CNOT , CZ , the Z -axis rotation gates $Z(\theta)$ and $ZZ(\theta)$, and the Toffoli gate, along with any gate which can be implemented by a sequence of bias-preserving gates. In what follows, we determine which bias-preserving gates are Pauli- Z compatible.

Proposition IV.2. The gates X , CZ , $Z(\theta)$, $ZZ(\theta)$, CNOT and SWAP are Pauli- Z compatible. The Toffoli gate is not Pauli- Z compatible.

Proof. The unitaries $X_{[i]}$, $\text{CZ}_{(i,j)}$ (with target qubit j), the Z -axis rotation unitaries $Z(\theta)$ and $ZZ(\theta)$, and any unitary $Z_{[A]}$ (for $A \subseteq \{1, \dots, n\}$), are bias-preserving unitary gates U such that $Z_i U = U Z_i$ for every index i , and therefore they are Pauli- Z compatible.

Additionally, the $\text{CNOT}_{(i,j)}$ gate (where we take j to be the target qubit) is such that

$$Z_{[i]} \text{CNOT}_{(i,j)} = \text{CNOT}_{(i,j)} Z_{[i]}, \quad (25)$$

$$\text{and } Z_{[i,j]} \text{CNOT}_{(i,j)} = \text{CNOT}_{(i,j)} Z_{[j]}, \quad (26)$$

as shown in Figure 2. Therefore, both the CNOT gate and the SWAP gate (when decomposed as 3 CNOT gates) are Pauli- Z compatible.

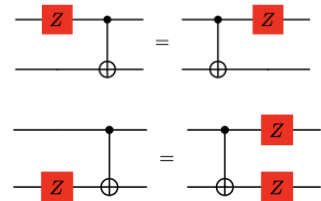


FIG. 2: Phase-flip propagation through the CNOT gate; the equality is between the unitaries associated to the circuits.

However, this is not the case for the Toffoli gate $\text{CCX}_{[i,j,k]}$ (with target qubit k), which is such that

$$Z_{[i]} \text{CCX}_{(i,j,k)} = \text{CCX}_{(i,j,k)} Z_{[i]}, \quad (27)$$

$$Z_{[j]} \text{CCX}_{(i,j,k)} = \text{CCX}_{(i,j,k)} Z_{[j]}, \quad (28)$$

$$\text{and } \text{CZ}_{(i,j)} Z_{[k]} \text{CCX}_{(i,j,k)} = \text{CCX}_{(i,j,k)} Z_{[k]}, \quad (29)$$

and is therefore not Pauli- Z compatible. \square

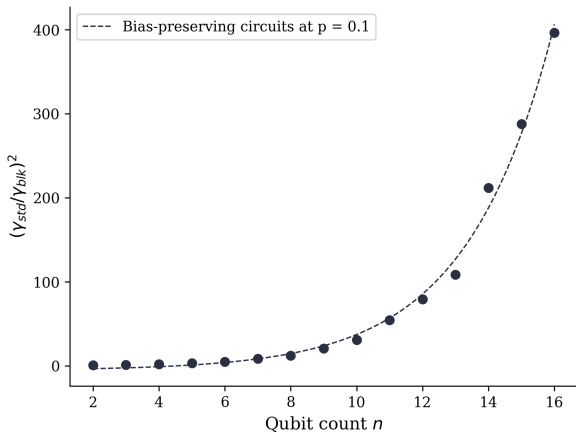


FIG. 3: Performance of Block-PEC on randomly generated bias-preserving circuits, at $p = 0.1$ uncorrelated dephasing noise; expressed as the sampling cost gain $(\gamma_{\text{std}}/\gamma_{\text{blk}})^2$ as a function of the qubit count n .

Hence, for circuits with Toffoli gates, it will be necessary to resort to Hybrid Block-PEC described earlier. Nonetheless, the gates listed in Proposition IV.2 form a generating set for a rather large class of (sub)-circuits on which one can implement Block-PEC.

b. Analytic performance guarantees. Additionally, we studied analytically all combinations of two bias-preserving gates acting on at most 2 qubits, subjected to uncorrelated dephasing noise. We found out that the per-block method leads to an improvement when a CNOT follows a gate which acts non-trivially on the CNOT's target qubit.

Proposition IV.3. *Assuming a non-zero 1-qubit phase flip error, Block-PEC yields a sampling cost reduction over PEC, on Pauli-Z compatible circuits with any sub-circuit of the form:*

$$(a) U_{(a)} = CNOT_{j,k}U_k;$$

$$(b) U_{(b)} = CNOT_{j,k}U_{j,k};$$

$$(c) U_{(c)} = CNOT_{i,j}U_{j,k} \text{ (with } i \neq k\text{)}.$$

Proof. Define p to be the 1-qubit phase flip error, and assume that $p > 0$. Let us write $\gamma_{\text{std}}(U)$ (resp. $\gamma_{\text{blk}}(U)$) for the sampling cost associated with the PEC (resp. Block-PEC) protocol for the circuit U . We represent these circuit patterns with their error locations in Figure 4. We refer to Appendix B for a definition of dephasing noise channels as linear combinations of Pauli-Z channels, and to Appendix E for the details of the calculations to follow.

For the circuit $U_{(a)} = CNOT_{j,k}U_k$, one can compute that

$$\gamma_{\text{blk}}(U_{(a)}) = |\beta_0| + 3|\beta_1| = \beta_0 - 3\beta_1, \quad (30)$$

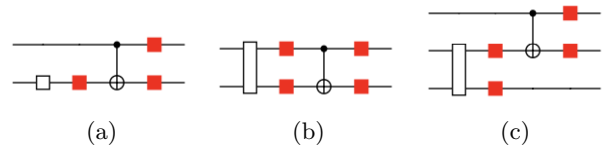


FIG. 4: Circuit $U_{(x)}$ with error locations, for $x \in \{a, b, c\}$.

with $\beta_0 = ((1-p)^3 - p^3)/(1-2p)^3$ and $\beta_1 = (p^2(1-p) - p(1-p)^2)/(1-2p)^3$. Then,

$$\gamma_{\text{blk}}(U_{(a)}) = \frac{1 + 2p - 2p^2}{(1-2p)^2} < \frac{1}{(1-2p)^3} = \gamma_{\text{std}}(U_{(a)}). \quad (31)$$

Similarly, one can compute that

$$\gamma_{\text{blk}}(U_{(b)}) = \frac{1 + 2p - 6p^2 + 4p^3}{(1-2p)^3} \quad (32)$$

$$< \frac{1}{(1-2p)^4} = \gamma_{\text{std}}(U_{(b)}), \quad (33)$$

$$\text{and } \gamma_{\text{blk}}(U_{(c)}) = \frac{1 + 2p - 2p^2}{(1-2p)^3} \quad (34)$$

$$< \frac{1}{(1-2p)^4} = \gamma_{\text{std}}(U_{(c)}). \quad (35)$$

□

The previous analysis can now be used to understand the possible gains for generic circuits that can be decomposed into sequences of sub-circuits with Pauli-Z compatible ones interspersed with non Pauli-Z compatible gates. Indeed, whenever the sub-circuits of the type $U_{(a)}, U_{(b)}, U_{(c)}$ appear within a circuit, Block-PEC yields an improvement over PEC (see Figure 5). The frequency of the appearance of such sub-circuits determines the efficiency of Block-PEC (see Figure 6 to see the improvement for randomly generated bias-preserving circuits). More concretely, if sub-circuits of type $U_{(a)}, U_{(b)}, U_{(c)}$ appear k times throughout the circuit, the sampling cost decreases by a factor proportional to kp^2 .

c. Performance evaluation for random circuits. To analyze the performance of Block-PEC for the gate set $\{X, Z, CNOT, Z(\theta), ZZ(\theta), CZ\}$, we have constructed random circuits acting on n qubits and with a maximum depth $n + 1$. More precisely, we have sampled uniformly at random $n + 1$ labels from the set $\{X, Z, CNOT, Z(\theta), ZZ(\theta), CZ\}$. For each label we have then randomly chosen the qubit(s) the corresponding gate has been acting upon. For $ZZ(\theta)$ gates, each angle θ has been chosen uniformly at random in $[0, 2\pi)$.

We then numerically evaluated the sampling cost gain (defined as the ratio $(\gamma_{\text{std}}/\gamma_{\text{blk}})^2$). It shows that for a noise strength of $p = 0.1$ and $n = 8$, the sampling overhead of PEC is more than twelve times that of Block-PEC, as shown in Figure 3. As expected, whenever the strength of the noise decreases, the difference between

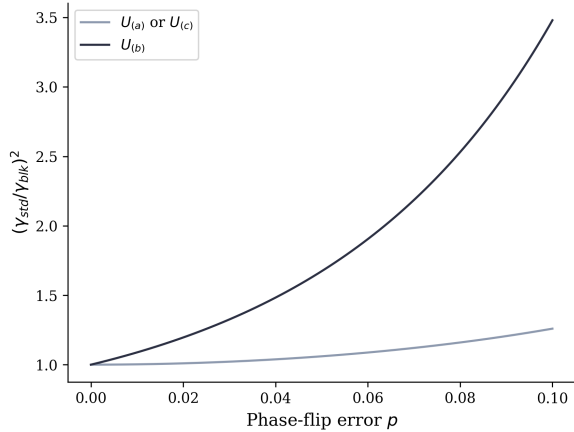


FIG. 5: Sampling cost gain $(\gamma_{\text{std}}/\gamma_{\text{blk}})^2$ for $U_{(x)}$ for $x \in \{a, b, c\}$, as a function of the uncorrelated phase-flip error p .

the two methods vanishes. Indeed, for low noise strength, the probability of having more than one error per circuit becomes small enough so that the noise is well approximated by first sampling a single layer within the block and then sampling an error for this layer. This effectively means that sampling per layer or per block will be equivalent up to negligible factors and hence yield a similar sampling overhead.

B. Partially bias-preserving circuits

a. Pauli-Z compatibility. As the definition of bias-preserving gates is quite restrictive, we have striven to identify gates which preserve phase flip biases but only on a subspace of the space of all quantum states. It is in this context that we studied parity-preserving gates. These gates are parameterized 2-qubit gates which perform a rotation in the subspace defined by $\text{span}\{|01\rangle, |10\rangle\}$, while acting as the identity on the rest. We define what it means for such a gate to be partially bias-preserving (see Appendix D for a complete mathematical characterization).

Definition IV.4. Consider \mathcal{S} to be a subspace of the Hilbert space of n quantum states. A gate is \mathcal{S} -bias-preserving if its unitary matrix representation G is:

1. stable under \mathcal{S} , i.e. $|\phi\rangle \in \mathcal{S} \implies G|\phi\rangle \in \mathcal{S}$;
2. such that for every n -by- n unitary diagonal matrix D , there is a n -by- n unitary diagonal matrix D' such that, for every state $|\phi\rangle \in \mathcal{S}$, $GD|\phi\rangle = D'G|\phi\rangle$.

RBS gates are 2-qubit rotation gates acting on $|01\rangle$ and

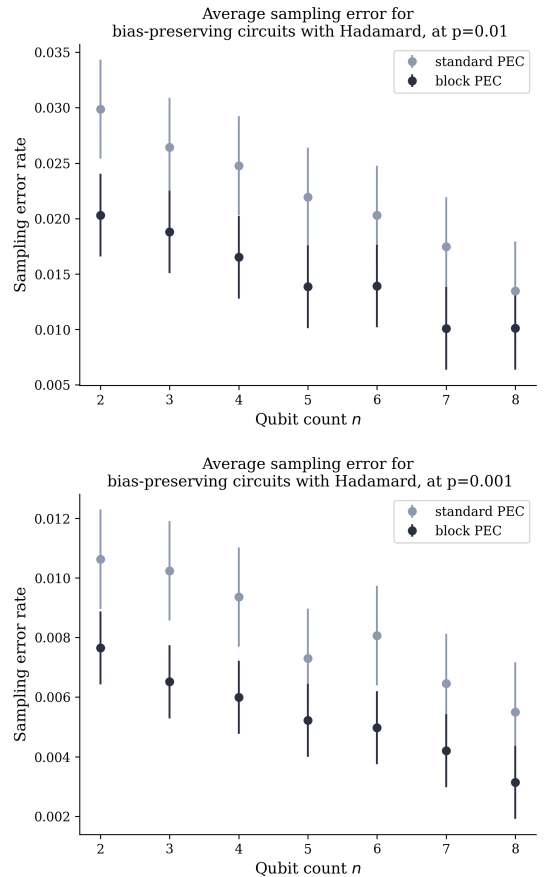


FIG. 6: Performance of Block-PEC under uncorrelated noise for randomly generated circuits, made of Pauli-Z compatible gates and Hadamard gates, in terms average sampling error rate (1000 samples per Monte Carlo simulation, with precision $\delta = 0.03$), over 1000 runs.

$|10\rangle$ as

$$RBS(\theta)|01\rangle = \cos(\theta)|01\rangle - \sin(\theta)|10\rangle \quad (36)$$

$$RBS(\theta)|10\rangle = \cos(\theta)|10\rangle + \sin(\theta)|01\rangle \quad (37)$$

while acting as the identity on $|00\rangle$ and $|11\rangle$.

We use parity-preserving gates, and in particular RBS gates, as examples of partially bias-preserving gates. Other examples of such partially bias-preserving parity-preserving gates are the $A(\theta, \phi)$ gate (see e.g. [4, 13, 14]), the Givens(θ) gate (see e.g. [2, 3, 21]), the $XY(\theta)$ gate (see e.g. [1]).

Theorem IV.5. RBS gates are partially bias-preserving gates.

Proof. See Appendix D. \square

The RBS gate can be implemented as the following sequence of three gates

$$RBS(\theta)_{j,k} = CNOT_{j,k}XCZ(\theta)_{j,k}CNOT_{j,k}, \quad (38)$$

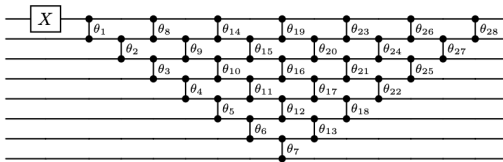


FIG. 7: 8-qubit pyramidal layering for matchgates.

where $XCZ(\theta)$ is the X -controlled $Z(\theta)$ rotation gate, represented by the unitary matrix

$$XCZ(\theta) = \frac{1}{2} \begin{pmatrix} 1 + e^{i\frac{\theta}{2}} & 0 & 1 - e^{i\frac{\theta}{2}} & 0 \\ 0 & 1 + e^{-i\frac{\theta}{2}} & 0 & 1 - e^{-i\frac{\theta}{2}} \\ 1 - e^{i\frac{\theta}{2}} & 0 & 1 + e^{i\frac{\theta}{2}} & 0 \\ 0 & 1 - e^{-i\frac{\theta}{2}} & 0 & 1 + e^{-i\frac{\theta}{2}} \end{pmatrix}.$$

Each of these gates is Pauli- Z compatible, making the 3-gate circuit implementing RBS Pauli- Z compatible.

b. Performance for RBS gate circuits. The previous decomposition of RBS gates contains the pattern $U_{(b)}$ as $XCZ(\theta)_{j,k}CNOT_{j,k}$. Therefore, as per the analysis of the previous subsection, one can expect non-trivial gains when using Block-PEC on algorithms which sample from RBS gate-based parameterized circuits.

We have numerically evaluated the 8-qubit pyramid represented in Figure 7 as it is a useful building block of several quantum machine learning algorithms (See Section V). Our simulations show that PEC requires more than 10 times as many quantum samples as Block-PEC when applied to a 8-qubit RBS diagonal (with randomly chosen RBS gate parameters) subjected to a phase-flip error probability of $p = 0.1$ (see Figure 9), thereby offering sizable advantage in using our technique for high noise strength.

V. BLOCK-PEC FOR CONCRETE APPLICATIONS

In this section, we consider multiple applications in the context of computational finance (Section V A) and machine learning (Section V B), and which fit in the framework defined by Block-PEC.

All numerical simulations were implemented in Python, using `Cirq` [9]. We use the `mitiq` library [22] to represent quasi-probabilistic distributions and execute the Monte Carlo simulations they correspond to. We implemented routines which pre-calculate the coefficients of Block-PEC's quasi-probabilistic distributions, for circuits subjected to dephasing noise,

For convenience, dephasing noise will be modeled by uncorrelated dephasing noise channels, as described in Appendix B. In practical implementations on cat-qubit architectures, dephasing noise is correlated. In Appendix E, we show that for circuits subjected to correlated dephasing noise, Block-PEC yields the same performance gains witnessed in Section IV A.

A. Mitigating errors in quantum option pricing

Option pricing is the task of estimating the payoff (value at expiration date) of option contracts. Building on quantum algorithms for amplitude estimation [15], Stamatopoulos et al. defined a family of quantum Monte Carlo algorithms for option pricing [27]. Such algorithms aim to calculate the expectation value of the payoff, by applying amplitude estimation to a unitary operator \mathcal{A} such that

$$\mathcal{A}|0\rangle^{\otimes(n+1)} = \sqrt{1-a}|\psi_0\rangle|0\rangle + \sqrt{a}|\psi_1\rangle|1\rangle \quad (39)$$

for some normalized states $|\psi_0\rangle$ and $|\psi_1\rangle$, where $a \in [0, 1]$ is the expectation value to estimate. The operator \mathcal{A} is formed by a data loading unitary $\mathcal{P}|0\rangle^{\otimes n} = \sum_x \sqrt{p_x}|x\rangle$ and a payoff unitary $\mathcal{R}|x\rangle|0\rangle = |x\rangle(\sqrt{f(x)}|1\rangle + \sqrt{1-f(x)}|0\rangle)$.

The unitary \mathcal{R} implements a piece-wise linear function $f: \{0, \dots, 2^n - 1\} \rightarrow [0, 1]_{\mathbb{R}}$ as

$$\mathcal{R}: |j\rangle|0\rangle \mapsto |j\rangle(\cos(f_j)|0\rangle + \sin(f_j)|1\rangle), \quad (40)$$

where $f_j = jf_1 + f_0$.

The term f_j is implemented by the j -th qubit, which controls a Y -rotation of angle $\theta_j = 2^j f_1$ on the ancilla qubit, at the exception f_0 which is implemented by a Y -rotation on the ancilla qubit. Y -rotations can be implemented as

$$Y(\theta) = SHZ(\theta)HS^\dagger \quad (41)$$

with the phase gate implemented as $S = Z(\pi/2)$, so that Y -rotations are implemented using only Pauli- Z compatible gates. Then, controlled Y -rotation can be implemented with only Pauli- Z compatible gates as

$$CY(\theta) = Y\left(\frac{\theta}{2}\right)_k CNOT_{j,k} Y\left(-\frac{\theta}{2}\right)_k CNOT_{j,k}. \quad (42)$$

We refer the interested reader to [27] for a detailed explanation of the definition of the angles θ_j in order to compute the expectation value of an option with payoff f .

The unitary \mathcal{R} is implemented by the circuit

$$\mathcal{R} = CY(\theta_n)_{n-1,n} \cdots CY(\theta_1)_{0,n} Y(\theta_0)_n. \quad (43)$$

Each implementation of $CY(\theta_j)$ (as in Equation 42) contains one circuit pattern $U_{(a)}$ as $Y\left(\pm\frac{\theta_j}{2}\right)_n CNOT_{j-1,n}$. With $n - 1$ repetitions of the circuit pattern $U_{(a)}$ in the implementation of \mathcal{R} , one can expect small gains when using Block-PEC as the sampling cost reduction for such sub-circuits is of lesser magnitude than for other types of sub-circuits.

To quantify the efficiency of Block-PEC on this algorithm, we simulated the mitigation of errors on the payoff unitary \mathcal{R} . The results of our numerical simulations are



FIG. 8: Average sampling error of PEC and Block-PEC on 4-qubit payoff functions, at $p = 0.01$ for uncorrelated noise; number of samples = 1000; sample variances: $\sigma_{\text{std}}^2 \simeq 5.05e^{-6}$, $\sigma_{\text{blk}}^2 \simeq 4.87e^{-6}$.

aggregated in Figure 8. We have simulated the mitigation of errors on 4-qubit payoff functions, implemented by the unitary $\mathcal{R}_4 = Y(\theta_0)CY(\theta_1)_{0,4} \cdots CY(\theta_4)_{3,4}$ for randomly chosen angles $\theta_0, \dots, \theta_4$. Taking $p = 10^{-2}$, we computed the average error of PEC and Block-PEC over 1000 samples. We observed that the sampling variance ratio is $\frac{\sigma_{\text{std}}^2}{\sigma_{\text{blk}}^2} \simeq 1.037548912$, which is in line with our expectation of a small sampling variance reduction when using Block-PEC over PEC.

B. RBS-based parameterized quantum circuits

In the use of RBS gates, a common construction involves executing RBS gates for various angles following a pyramidal structure, as shown in Figure 7.

For example, any orthogonal neural network can be mapped onto a pyramid of RBS gates acting on unary states [20]. The training time of quantum (orthogonal) neural networks is in $O(1/\varepsilon^2)$, where ε is the accuracy of the estimation of the circuit's output. Mitigating errors increases accuracy, and therefore reduces training time.

It is worth noting that using a unary encoding allows to detect errors by discarding non-unary output states, which can only appear when a bit flip occurred during the computation. While efficient, this is a potentially costly strategy. A low bit-flip error rate architecture makes the cost of this non-unary state error detection strategy negligible.

The sampling cost improvement that Block-PEC yields for RBS-based parameterized quantum circuits depends on the particular architecture considered and the implementation of RBS gates. And since the calculation of the coefficients of the quasi-probabilistic distributions for Block-PEC does not depend on the angles of RBS gates, it is sufficient to calculate them once for every RBS-based parameterized circuit architecture, reducing the classical overhead of our Block-PEC approach.

This observation has multiple consequences. First, applying this reasoning to Noise-Extended PEC (NEPEC) [23], which generalizes both PEC and Zero-Noise Extrapolation (ZNE), one can observe that mitigating errors by anti-diagonals is also an efficient strategy in the context of ZNE.

Secondly, anti-diagonals of RBS gates can be used to implement a unary data loader for the quantum option

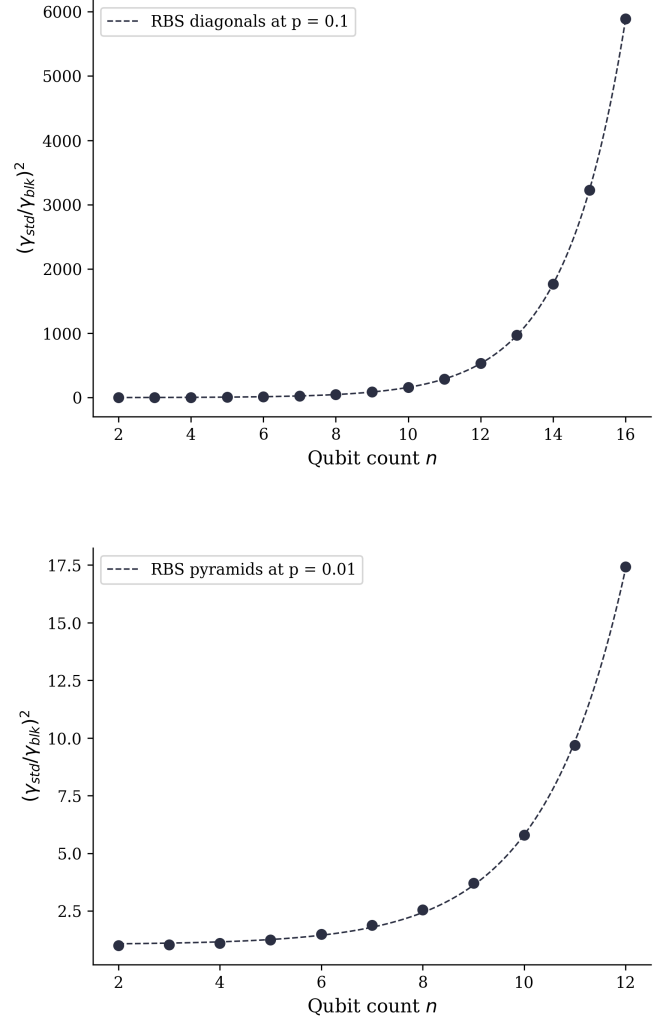


FIG. 9: Performance of Block-PEC on diagonals and pyramids of RBS gates, at $p = 0.1$ and $p = 0.01$ respectively for uncorrelated noise; expressed as the sampling cost gain $(\gamma_{\text{std}}/\gamma_{\text{blk}})^2$ as a function of the qubit count n .

pricing algorithm, as presented in [25]. Then Block-PEC yields an improvement over PEC on the entire execution of unary option pricing, and not just on the sub-circuit corresponding to the payoff function.

We observed that PEC requires more than twice as many quantum samples as Block-PEC when applied to a 8-qubit RBS pyramid subjected to a phase-flip error probability of $p = 0.01$, as show in Figure 9.

Since each implementation of $RBS(\theta)$ (as in Equation 42) contains one circuit pattern $U_{(b)}$ as $XCZ(\theta)_{j,k}CNOT_{j,k}$, one can expect noticeable gains when using Block-PEC. To quantify the efficiency of Block-PEC on this algorithm, we simulated the mitigation of errors on 4-qubit RBS pyramids at $p = 10^{-2}$. We computed the average error of PEC and Block-PEC over 1000 samples. We observed that the sampling variance



FIG. 10: Average sampling error of PEC and Block-PEC on 4-qubit RBS pyramids at $p = 10^{-2}$ for uncorrelated noise; number of samples = 1000; sample variances: $\sigma_{\text{std}}^2 \simeq 3.51e^{-14}$, $\sigma_{\text{blk}}^2 \simeq 2.08e^{-14}$.

ratio is $\frac{\sigma_{\text{std}}^2}{\sigma_{\text{blk}}^2} \simeq 1.684731146$, which suggests a noticeable improvement of the sampling variance when using Block-PEC (see Figure 10).

VI. CONCLUSION

We have introduced Block-PEC, a variation of the probabilistic error cancellation for error mitigation that takes into account the specifics of the noise model and the propagation of errors to lower the overhead of using noisy quantum computers in lieu of perfect ones. The model that we consider, is that of biased noise qubits as implemented by superconducting cat-qubit architectures.

Our technique provides a provable advantage for circuits where several bias-preserving gates follow one another. It constructs an aggregate noise model that can be inverted all at once instead of a per gate basis. This results in a lower sampling cost for achieving a given precision at the cost of classical pre-computation.

We performed numerical simulations for assessing typical performance on two classes of circuits: first for circuits made of random one and two-qubit bias-preserving gates, and second for specific arrangements of RBS gates. In accordance with our theoretical results, Block-PEC is

most efficient for deeper circuits, as the cost of the classical pre-computation increases exponentially with the width of the circuit but only linearly with its depth. For example, for 8-qubit RBS diagonals (at $p = 0.1$) and 8-qubit RBS pyramids (at $p = 0.01$), the overhead is divided by a factor of at least 10 and 2 respectively.

Using these simulation results, we argued that for applications such as option pricing or orthogonal neural networks, Block-PEC leads to a reduction of the sampling variance.

We have shown that this advantage carries over whenever sub-circuits made out of several bias-preserving gates can be identified within the full computation. This is possible by performing a hybrid simulation of the full circuit. The bias-preserving sub-circuits are sampled according to the aggregate noise model defined by Block-PEC while the other gates are simply sampled according to the regular PEC technique. Then, one run of the hybrid simulation corresponds to independently sampling each of the sub-circuits and non bias-preserving gates.

This work also exemplifies that cat-qubits architectures can be advantageous to use in the NISQ-regime thanks to their noise model that can be more efficiently handled by error mitigation techniques. As such this raises two related questions: what other error mitigation techniques can benefit from bias noise qubits and, more generally, are there architectures for which error mitigation techniques can be tailored and made particularly efficient?

Acknowledgements. This research was supported by Région Île-de-France under project QML-CAT agreement 22002432 PAQ 2022. The authors would like to thank Jérémie Guillaud and Romain Kukla for numerous fruitful discussions during project meetings. The authors are grateful to the CLEPS infrastructure from INRIA Paris for providing resources and support in obtaining the numerical results reported here.

-
- [1] ABRAMS, D. M., DIDIER, N., JOHNSON, B. R., SILVA, M. P. D., AND RYAN, C. A. Implementation of xy entangling gates with a single calibrated pulse. *Nature Electronics* 3, 12 (Nov. 2020), 744–750.
- [2] ANSEMETTI, G.-L. R., WIERICHS, D., GOGOLIN, C., AND PARRISH, R. M. Local, expressive, quantum-number-preserving vqe ansätze for fermionic systems. *New Journal of Physics* 23, 11 (Nov. 2021), 113010.
- [3] ARUTE, F., ARYA, K., BABBUSH, R., BACON, D., BARDIN, J. C., BARENDTS, R., BENGTTSSON, A., BOIXO, S., BROUGHTON, M., BUCKLEY, B. B., BUELL, D. A., BURKETT, B., BUSHNELL, N., CHEN, Y., CHEN, Z., CHEN, Y.-A., CHIARO, B., COLLINS, R., COTTON, S. J., COURTNEY, W., DEMURA, S., DERK, A., DUNSWORTH, A., EPPENS, D., ECKL, T., ERICKSON, C., FARHI, E., FOWLER, A., FOXEN, B., GIDNEY, C., GIUSTINA, M., GRAFF, R., GROSS, J. A., HABEGGER, S., HARRIGAN, M. P., HO, A., HONG, S., HUANG, T., HUGGINS, W., IOFFE, L. B., ISAKOV, S. V., JEFFREY, E., JIANG, Z., JONES, C., KAFRI, D., KECHEDZHI, K., KELLY, J., KIM, S., KLIMOV, P. V., KOROTKOV, A. N., KOSTRITSA, F., LANDHUIS, D., LAPTEV, P., LINDMARK, M., LUCERO, E., MARTHALER, M., MARTIN, O., MARTINIS, J. M., MARUSCZYK, A., MCARDLE, S., MCCLEAN, J. R., MCCOURT, T., MCEWEN, M., MEGRANT, A., MEJUTO-ZAERA, C., MI, X., MOHSENI, M., MRUCZKIEWICZ, W., MUTUS, J., NAAMAN, O., NEELEY, M., NEILL, C., NEVEN, H., NEWMAN, M., NIU, M. Y., O'BRIEN, T. E., OSTBY, E., PATÓ, B., PETUKHOV, A., PUTTERMAN, H., QUINTANA, C., REINER, J.-M., ROUSHAN, P., RUBIN, N. C., SANK, D., SATZINGER, K. J., SMELYANSKIY, V., STRAIN, D., SUNG, K. J., SCHMITTECKERT, P., SZALAY, M., TUBMAN, N. M., VAINSENER, A., WHITE, T., VOGT, N., YAO, Z. J., YEH, P., ZALCMAN, A., AND ZANKER, S. Observation of separated dynamics of charge and spin in the fermi-hubbard model, 2020.
- [4] BARKOUTSOS, P. K., GONTHIER, J. F., SOKOLOV, I., MOLL, N., SALIS, G., FUHRER, A., GANZHORN, M.,

- EGGER, D. J., TROYER, M., MEZZACAPO, A., FILIPP, S., AND TAVERNELLI, I. Quantum algorithms for electronic structure calculations: Particle-hole Hamiltonian and optimized wave-function expansions. *Physical Review A* 98, 2 (Aug. 2018).
- [5] BERDOU, C., MURANI, A., REGLADE, U., SMITH, W., VILLIERS, M., PALOMO, J., ROSTICHER, M., DENIS, A., MORFIN, P., DELBECQ, M., KONTOS, T., PANKRATOVA, N., RAUTSCHKE, F., PERONNIN, T., SELLEM, L.-A., ROUCHON, P., SARLETTE, A., MIRRAHIMI, M., CAMPAGNE-IBARCQ, P., JEZOUIN, S., LESCANNE, R., AND LEGHTAS, Z. One hundred second bit-flip time in a two-photon dissipative oscillator. *PRX Quantum* 4, 2 (jun 2023).
- [6] CAI, Z., BABBUSH, R., BENJAMIN, S. C., ENDO, S., HUGGINS, W. J., LI, Y., MCCLEAN, J. R., AND O'BRIEN, T. E. Quantum error mitigation. *Reviews of Modern Physics* 95, 4 (Dec. 2023).
- [7] CHERRAT, E. A., KERENIDIS, I., MATHUR, N., LANDMAN, J., STRAHM, M., AND LI, Y. Y. Quantum vision transformers, 2022.
- [8] CHERRAT, E. A., RAJ, S., KERENIDIS, I., SHEKHAR, A., WOOD, B., DEE, J., CHAKRABARTI, S., CHEN, R., HERMAN, D., HU, S., MINNSEN, P., SHAYDULIN, R., SUN, Y., YALOVETZKY, R., AND PISTOIA, M. Quantum deep hedging, 2023.
- [9] DEVELOPERS, C. Cirq, May 2024.
- [10] ENDO, S., BENJAMIN, S. C., AND LI, Y. Practical quantum error mitigation for near-future applications. *Physical Review X* 8, 3 (jul 2018).
- [11] ENDO, S., BENJAMIN, S. C., AND LI, Y. Practical quantum error mitigation for near-future applications. *Phys. Rev. X* 8 (Jul 2018), 031027.
- [12] ENDO, S., CAI, Z., BENJAMIN, S. C., AND YUAN, X. Hybrid quantum-classical algorithms and quantum error mitigation. *Journal of the Physical Society of Japan* 90, 3 (Mar. 2021), 032001.
- [13] FILIP, M.-A., RAMO, D. M., AND FITZPATRICK, N. Variational Phase Estimation with Variational Fast Forwarding. *Quantum* 8 (Mar. 2024), 1278.
- [14] GARD, B. T., ZHU, L., BARRON, G. S., MAYHALL, N. J., ECONOMOU, S. E., AND BARNES, E. Efficient symmetry-preserving state preparation circuits for the variational quantum eigensolver algorithm. *npj Quantum Information* 6, 1 (Jan. 2020).
- [15] GIURGICA-TIRON, T., JOHRI, S., KERENIDIS, I., NGUYEN, J., PISENTI, N., PRAKASH, A., SOSNOVA, K., WRIGHT, K., AND ZENG, W. Low depth amplitude estimation on a trapped ion quantum computer, 2021.
- [16] GUILLAUD, J., COHEN, J., AND MIRRAHIMI, M. Quantum computation with cat qubits. *arXiv preprint arXiv:2203.03222* (2022).
- [17] JAIN, N., LANDMAN, J., MATHUR, N., AND KERENIDIS, I. Quantum Fourier Networks for Solving Parametric PDEs, 2023.
- [18] JOHRI, S., DEBNATH, S., MOCHERLA, A., SINGH, A., PRAKASH, A., KIM, J., AND KERENIDIS, I. Nearest centroid classification on a trapped ion quantum computer, 2020.
- [19] JONES, B. D. M., LINDEN, N., AND SKRZYPCZYK, P. The hadamard gate cannot be replaced by a resource state in universal quantum computation, 2024.
- [20] KERENIDIS, I., LANDMAN, J., AND MATHUR, N. Classical and quantum algorithms for orthogonal neural networks, 2022.
- [21] KIVLICHAN, I. D., MCCLEAN, J., WIEBE, N., GIDNEY, C., ASPURU-GUZI, A., CHAN, G. K.-L., AND BABBUSH, R. Quantum simulation of electronic structure with linear depth and connectivity. *Physical Review Letters* 120, 11 (Mar. 2018).
- [22] LAROSE, R., MARI, A., KAISER, S., KARALEKAS, P. J., ALVES, A. A., CZARNIK, P., EL MANDOUH, M., GORDON, M. H., HINDY, Y., ROBERTSON, A., ET AL. Mitiq: A software package for error mitigation on noisy quantum computers. *Quantum* 6 (2022), 774.
- [23] MARI, A., SHAMMAH, N., AND ZENG, W. J. Extending quantum probabilistic error cancellation by noise scaling. *Physical Review A* 104, 5 (nov 2021).
- [24] MONTANARO, A. Quantum speedup of Monte Carlo methods. *Proceedings of the Royal Society A: Mathematical, Physical and Engineering Sciences* 471, 2181 (Sept. 2015), 20150301.
- [25] RAMOS-CALDERER, S., PÉREZ-SALINAS, A., GARCÍA-MARTÍN, D., BRAVO-PIRETO, C., CORTADA, J., PLANAGUMÀ, J., AND LATORRE, J. I. Quantum unary approach to option pricing. *Physical Review A* 103, 3 (Mar. 2021).
- [26] RÉGLADE, U., BOCQUET, A., GAUTIER, R., MARQUET, A., ALBERTINALE, E., PANKRATOVA, N., HALLÉN, M., RAUTSCHKE, F., SELLEM, L.-A., ROUCHON, P., SARLETTE, A., MIRRAHIMI, M., CAMPAGNE-IBARCQ, P., LESCANNE, R., JEZOUIN, S., AND LEGHTAS, Z. Quantum control of a cat-qubit with bit-flip times exceeding ten seconds, 2023.
- [27] STAMATOPOULOS, N., EGGER, D. J., SUN, Y., ZOUFAL, C., ITEN, R., SHEN, N., AND WOERNER, S. Option pricing using quantum computers. *Quantum* 4 (July 2020), 291.
- [28] STRIKIS, A., QIN, D., CHEN, Y., BENJAMIN, S. C., AND LI, Y. Learning-based quantum error mitigation. *PRX Quantum* 2, 4 (Nov. 2021).
- [29] TAKAGI, R. Optimal resource cost for error mitigation. *Physical Review Research* 3, 3 (aug 2021).
- [30] TAKAGI, R., ENDO, S., MINAGAWA, S., AND GU, M. Fundamental limits of quantum error mitigation. *npj Quantum Information* 8, 1 (sep 2022).
- [31] TEMME, K., BRAVYI, S., AND GAMBETTA, J. M. Error mitigation for short-depth quantum circuits. *Physical Review Letters* 119, 18 (nov 2017).
- [32] TRAN, M. C., SHARMA, K., AND TEMME, K. Locality and error mitigation of quantum circuits, 2023.
- [33] VAN DEN BERG, E., MINEV, Z. K., KANDALA, A., AND TEMME, K. Probabilistic error cancellation with sparse pauli-lindblad models on noisy quantum processors. *Nature Physics* 19, 8 (May 2023), 1116–1121.

Appendix A: A primer in probabilistic error cancellation

Quantum error mitigation techniques aim to minimize the estimation bias when sampling from noisy circuits. The Probabilistic Error Cancellation (PEC [31]) approach performs a Monte Carlo simulation of the inverse of the noise model, in order to remove this estimation bias: from a generating set of noisy (implementable)

gates, the inverted noise model is approximated as a linear combination of noisy gates. Therefore, bounds on the sampling cost of PEC are tied to the quality of available physical implementations.

The Monte Carlo sampling is applied for a given circuit $U = U_d \circ \dots \circ U_1$ formed by d gates where each ideal gate U_l is decomposed as the linear combination of implementable noisy gates

$$U_l = \gamma_l \sum_{1 \leq j \leq J} p_{j,l} s_{j,l} \widetilde{B}_{j,l}, \quad (\text{A1})$$

and under the assumption that $p_j = |\alpha_{j,l}|/\gamma_l$, $\gamma_l = \sum_j |\alpha_{j,l}|$ and $s_{j,l} \in \{-1, 1\}$ are efficiently computable.

This stochastic simulation operates as follows:

1. Sample a noisy gate $\widetilde{B}_{j,l}$ for each ideal gate U_l with probability $p_{j,l}$;
2. Execute the circuit corresponding to the channels $\widetilde{B}_{j,d} \dots \widetilde{B}_{j,1}$, and measure the observable O , obtaining outcome o ;
3. Multiply the outcome o by $\gamma_{\text{total}} = \prod_l \gamma_l$ and $\text{sgn}_{\text{total}} = \prod_j s_j$;
4. Repeat those three steps S times and compute the average μ of the product o .

In this stochastic simulation, an unbiased estimator of U_l is given by

$$\widehat{U}_l = \gamma_l s_{j,l} \widetilde{B}_{j,l}, \quad (\text{A2})$$

with variance $O(\gamma_l^2)$, so that an unbiased estimator of U is given by

$$\widehat{U}_d \dots \widehat{U}_1 = \gamma_{\text{total}} \text{sgn}_{\text{total}} \widetilde{B}_{j,d} \dots \widetilde{B}_{j,1}, \quad (\text{A3})$$

with variance $O(\gamma_{\text{total}}^2)$.

In other words, the stochastic simulation aims to approximate the expectation value $\langle O \rangle_{\text{ideal}} = \text{Tr}[OU(\rho_0)]$ for some observable O , given the initial state $\rho_0 = |0\rangle\langle 0|^{\otimes n}$. From the quasi-probabilistic distribution defined in Equation A1, the expectation value of U can be calculated from the expectation value

$$\langle O \rangle_{j_1, \dots, j_d} = \text{Tr}\left[O \widetilde{B}_{j_d} \dots \widetilde{B}_{j_1}(\rho_0)\right] \quad (\text{A4})$$

of the noisy gates $\widetilde{B}_{j_d}, \dots, \widetilde{B}_{j_1}$, that is

$$\langle O \rangle_{\text{ideal}} = \sum_{j_1, \dots, j_d} \alpha_{j_1} \dots \alpha_{j_d} \langle O \rangle_{j_1, \dots, j_d}. \quad (\text{A5})$$

It is the sampling cost γ_{total} which determines the efficiency of PEC as a quantum error mitigation approach.

Hoeffding's inequality states that the probability that the estimate μ differs from the true mean value by more than $\delta > 0$ is at most $2 \exp\left(-\frac{2S\delta^2}{\gamma_{\text{total}}^2}\right)$, so that the sample

average deviates from the true mean value with variance $\sigma^2 \in O\left(\frac{\gamma_{\text{total}}^2}{S\delta^2}\right)$. Thus the number of samples S required to attain precision $\delta > 0$, with probability at least $1 - \varepsilon$, is

$$S \geq \frac{\gamma_{\text{total}}^2}{2\delta^2} \ln\left(\frac{2}{\varepsilon}\right). \quad (\text{A6})$$

1. Solving the noise inversion equation

Consider the noisy layered circuit

$$\widetilde{U} = \widetilde{U}_d \circ \dots \circ \widetilde{U}_1 \quad (\text{A7})$$

defined by a succession of implementable noisy gates, which each satisfy the equality $\widetilde{U}_l = N_l \circ U_l$, where N_l is the noise map associated to the gate U_l .

Now, assuming that \widetilde{U}_l and U_l are known, one can express the inverse $N_l^{-1} = U_l \circ \widetilde{U}_l^{-1}$ of the noise map, as a linear combination of unitary channels and preparation channels

$$N_l^{-1} = \sum_j \alpha_{j,l} V_{j,l}, \quad (\text{A8})$$

so that each unitary U_l can be rewritten as

$$U_l = N_l \circ N_l^{-1} \circ U_l = \sum_j \alpha_{j,l} \widetilde{B}_{j,l}, \quad (\text{A9})$$

We define $\widetilde{B}_{j,l} = N_l \circ V_{j,l} \circ U_l$ to be the noisy gate associated to each unitary/preparation channel $V_{j,l}$.

The inverse N_l^{-1} of the noise channel can easily be obtained by observing that determining coefficients $\alpha_{j,l}$ such that Equation A8 holds means solving the equation

$$I^{\otimes n_l} = N_l \circ \sum_j \alpha_{j,l} V_{j,l}, \quad (\text{A10})$$

where n_l is the number of qubits on which the operator U_l acts non-trivially.

2. Parameters influencing the sampling cost

Minimizing the number of samples needed means solving the following Linear Program (LP) for each U_l (which acts non-trivially on n_l qubits):

$$\begin{aligned} & \text{minimize} \sum_{j=1}^J |\alpha_j| \\ & \text{subject to } U_l = \sum_{1 \leq j \leq J} \alpha_j \widetilde{B}_{j,l}, \end{aligned} \quad (\text{A11})$$

where all the noisy implementable unitary operations $\widetilde{B}_{j,l}$ are in the support of U_l (as a linear combination), assuming that U_l has a non-trivial support and on few qubits.

We take the solution (if feasible) of this LP to be γ_{n_l} , so that $p_j = \frac{|\alpha_j|}{\gamma_{n_l}}$ and $s_j = \text{sgn}(\alpha_j)$.

We do so for all U_l , so that U is obtained as a product of the solutions of the LPs:

$$U = \gamma_{\text{total}} \sum_{j_1, \dots, j_d} \alpha_{j_1, \dots, j_d} \widetilde{B}_{j_d, d} \cdots \widetilde{B}_{j_1, 1}, \quad (\text{A12})$$

with $\gamma_{\text{total}} = \gamma_{n_d} \cdots \gamma_{n_1}$ and $\alpha_{j_1, \dots, j_d} = \alpha_{j_d} \cdots \alpha_{j_1}$, where $\alpha_{j_l} = p_{j_l} s_{j_l} \gamma_{n_l}$ for each j_l , so that $p_{j_1, \dots, j_d} = p_{j_d} \cdots p_{j_1}$ and $s_{j_1, \dots, j_d} = s_{j_d} \cdots s_{j_1}$.

Appendix B: Dephasing noise channels

In the present work, dephasing noise channels are linear combinations of Pauli- Z channels. A dephasing noise channel over a set of qubits A can be mathematically represented as linear combination $\sum_{B \subseteq A} \text{prob}(B) Z_{[B]}$ of Pauli quantum channels $Z_{[B]}$ (where prob is a probability distribution over the partition of A), associated to the Pauli unitary $Z_{[B]}$ defined for $B \subseteq A$ by

$$Z_{[B]} = \left(\bigotimes_{i \in B} Z_i \right) \otimes \left(\bigotimes_{i \in A \setminus B} I_i \right), \quad (\text{B1})$$

so that $Z_\emptyset = I^{\otimes n}$, and $m = |A|$ is the number of qubits on which Z_A acts non-trivially.

1. Inverting uncorrelated dephasing noise

Typically (see e.g. [30]), uncorrelated dephasing noise channels are defined over a set of qubits A as

$$F_p^{[A]} = \bigotimes_{j \in A} ((1-p)I_j + pZ_j) \quad (\text{B2})$$

Now, observe that $F_p^{[A]}$ can be rewritten as

$$F_p^{[A]} = \sum_{B \subseteq A: |B|=m} (1-p)^{n-m} p^m Z_{[B]}, \quad (\text{B3})$$

The inverted noise channel $(F_p^{\{\{j\}\}})^{-1}$ on one qubit is given by

$$(F_p^{\{\{j\}\}})^{-1} = \gamma_1 ((1-p)I_j - pZ_j) \quad (\text{B4})$$

for $\gamma_k = \frac{1}{(1-2p)^k}$.

Then, for an arbitrary qubit set A of size n , we define the inverted noise channel $(F_p^{[A]})^{-1}$ by

$$\begin{aligned} (F_p^{[A]})^{-1} &= \gamma_n \left(\bigotimes_{j \in A} ((1-p)I_j - pZ_j) \right) \\ &= \gamma_n \sum_{B \subseteq A: |B|=m} (1-p)^{n-m} (-p)^m Z_{[B]}. \end{aligned} \quad (\text{B5})$$

One can verify that

$$\begin{aligned} \gamma_{\text{total}} &= \gamma_n \sum_{m=0}^n p^m (1-p)^{n-m} \binom{n}{m} \\ &= \gamma_n 1 = \gamma_1^n. \end{aligned} \quad (\text{B6})$$

2. Approximating impure dephasing noise

Let us justify our use of a pure dephasing noise model, instead of a model which allows for some depolarizing noise. For simplification we omit in this section the indices of the qubits that noise channels are defined on.

Consider the local depolarizing noise model given by

$$D_p^{(1)} = (1-p)I + \frac{p}{3}(X+Y+Z), \text{ and } D_p^{(n)} = (D_p^{(1)})^{\otimes n}. \quad (\text{B7})$$

One can define an impure local dephasing noise model, which allows for some depolarizing noise, as the noise channels given for any $q \geq 0$ by

$$L_{p,q}^{(1)} = (1-p)I + p \left(\frac{q}{q+1} Z + \frac{1}{3} \frac{1}{q+1} (X+Y+Z) \right), \quad (\text{B8})$$

$$L_{p,q}^{(n)} = (L_{p,q}^{(1)})^{\otimes n}, \quad (\text{B9})$$

so that $L_{p,q}^{(n)}$ is the local depolarizing noise for $q=0$ and the local dephasing noise when q tends to infinity.

The distance between the quantum channels $F_p^{(1)}$ and $L_{p,q}^{(1)}$ is defined as the diamond norm of their difference, which is such that

$$\|F_p^{(1)} - L_{p,q}^{(1)}\|_\diamond = \frac{2p}{3(q+1)} \left\| Z - \frac{1}{2}(X+Y) \right\|_\diamond. \quad (\text{B10})$$

Therefore, the bias incurred by the impure dephasing noise model, quantified as the distance between the pure and impure dephasing noise channels, is proportional to $\frac{2p}{3(q+1)}$.

Observing that

$$(F_p^{(1)})^{-1} = \gamma_1 ((1-p)I - pZ), \quad (\text{B11})$$

$$\begin{aligned} (L_{p,q}^{(1)})^{-1} &= \gamma_1 \left((1-p)I - p \frac{3q+1}{3(q+1)} Z \right. \\ &\quad \left. - p \frac{1}{3(q+1)} (X+Y) \right), \end{aligned} \quad (\text{B12})$$

with $\gamma_1 = \frac{1}{1-2p}$, it follows that the distance $\left\| (F_p^{(1)})^{-1} - (L_{p,q}^{(1)})^{-1} \right\|_\diamond$ between the pure and impure dephasing inverted noise channels is proportional to $\gamma_1 \frac{2p}{3(q+1)}$.

For cat-qubit architectures, the effective bit flip rate is proportional to $e^{-c\bar{n}}$ where c is a constant and \bar{n} is the

mean number of photons (the ‘‘cat size’’), which comes at the cost of a higher phase flip rate, with a rate increase proportional to \bar{n} [16].

For a realistic description of the noise model of cat-qubit architectures, one could take the noise channel $\mathbf{L}_{p,q}^{(1)}$ with $q = \frac{e^{c\bar{n}}}{\bar{n}} - 1$, so that $\frac{1}{q+1} = \bar{n}e^{-c\bar{n}}$. However, for $c = 2$, q is of the order of 10^3 and 10^7 for \bar{n} equal to 5 and 10 respectively (which are both reasonable values for \bar{n} under current experiments [5, 16, 26]). Therefore, in the context of PEC-like error mitigation protocols, pure dephasing noise channels constitute a good approximation of the noise associated to bias-preserving circuits implemented on cat-qubits.

Appendix C: Bias-preserving gates

Informally, bias-preserving gates are quantum gates which have the property that they do not turn phase-flip errors into bit-flip errors. In other words, phase-flip errors are mapped to phase-flip errors, preserving phase-flip biases. We show that bias-preserving gates have matrix representations which can be described as generalized permutation matrices.

Definition C.1. *A n -qubit gate is bias-preserving if its unitary matrix representation G is such that for every n -by- n unitary diagonal matrix D , there is a n -by- n unitary diagonal matrix D' such that $GDG^\dagger = D'$, i.e. $GD = D'G$.*

In other words, a n -qubit gate is bias-preserving if its matrix representation is in the normalizing group $N(\mathcal{D}_n)$ of the group \mathcal{D}_n of n -by- n unitary diagonal matrices. To characterize $N(\mathcal{D}_n)$, we introduce the notion of generalized permutation matrix.

Definition C.2. *A generalized permutation matrix is a matrix such that each column/row has exactly one non-zero entry.*

Generalized permutation matrices are known to be the normalizer of diagonal matrices, that is, they form the largest subgroup of $GL_n(\mathbb{C})$ such that diagonal matrices are normal (i.e. for every $g \in GL_n(\mathbb{C})$, if d is a n -by- n diagonal matrix then so does gdg^\dagger). Considering unitary matrices within this context leads to the following proposition.

Proposition C.3. *A gate is bias-preserving if its matrix representation is in $N(\mathcal{D}_n) = \mathcal{P}_n\mathcal{D}_n$.*

Proof. Elements of the group $N(\mathcal{D}_n)$ are unitary generalized permutation matrices. Observe that for every generalized permutation n -by- n matrix M , there is a permutation $\sigma \in S_n$ and a complex vector $m = (m_1, \dots, m_n) \in \mathbb{C}^n$ such that

$$M_{i,j} = \begin{cases} m_j & \text{if } i = \sigma(j) \\ 0 & \text{otherwise.} \end{cases} \quad (\text{C1})$$

Now, consider two generalized permutation matrices M and M' , respectively characterized by the pairs (σ, m) and (σ', m') . Then the multiplication of M by M' is given componentwise by

$$(MM')_{i,j} = \begin{cases} m_{\sigma'(j)}m'_j & \text{if } i = \sigma\sigma'(j) \\ 0 & \text{otherwise.} \end{cases} \quad (\text{C2})$$

Writing $M_{\sigma,m}$ for the generalized permutation matrix characterized by the permutation σ and the complex vector m , we observe that

$$M_{\sigma,m} = M_{\sigma,(1,\dots,1)}M_{\text{id},m} \quad (\text{C3})$$

where $M_{\sigma,(1,\dots,1)}$ is a permutation and $M_{\text{id},m}$ is a diagonal matrix. In other words, every generalized permutation matrix is the product of a permutation and a diagonal matrix. This statement is in particular true for unitary generalized permutation matrices, for which the characteristic vector m is such that $m_j \neq 0$ and $m_j\bar{m}_j = 1$ (since the eigenvalues of any unitary matrix have modulus 1). \square

To put it simply, bias-preserving gates are normalizers of diagonal matrices in the group of unitary matrices. This normalizer is fully characterized by products of permutation matrices and diagonal unitaries.

Appendix D: Partially bias-preserving gates

This section recalls the definition of partially bias-preserving gates, introduces RBS gates, before giving a detailed proof that RBS gates are partially bias-preserving.

Definition D.1. *Consider \mathcal{S} to be a subspace of the Hilbert space of n quantum states. A gate is \mathcal{S} -bias-preserving if its unitary matrix representation G is:*

1. *stable under \mathcal{S} , i.e. $|\phi\rangle \in \mathcal{S} \implies G|\phi\rangle \in \mathcal{S}$;*
2. *such that for every n -by- n unitary diagonal matrix D , there is a n -by- n unitary diagonal matrix D' such that, for every state $|\phi\rangle \in \mathcal{S}$, $GD|\phi\rangle = D'G|\phi\rangle$.*

A natural strategy for error mitigation when sampling from such gates is to exclude measurement outcomes which do not belong to the set \mathcal{S} (i.e. measurement outcomes which are not of the form $\sum_j \alpha_j |\phi_j\rangle$ for $|\phi_j\rangle \in \mathcal{S}$), and then apply the same error mitigation strategies that we develop for bias-preserving gates.

1. Reconfigurable Beam Splitter (RBS) gates

The RBS (Reconfigurable Beam Splitter) gate is a gate which performs a rotation in the Hilbert space spanned

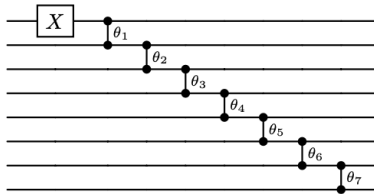


FIG. 11: Unary data loaders on 8 qubits (diagonal)

by the unit vector $|01\rangle$ and $|10\rangle$, so that

$$RBS(\theta) |01\rangle = \cos(\theta) |01\rangle - \sin(\theta) |10\rangle \quad (D1)$$

$$RBS(\theta) |10\rangle = \cos(\theta) |10\rangle + \sin(\theta) |01\rangle \quad (D2)$$

while acting as the identity on $|00\rangle$ and $|11\rangle$.

This RBS gate is particularly useful when its input subspace is restricted to states of Hamming distance 1, as the RBS gate preserves this property. The gate $iRBS$ shares the same properties, since the gate $iRBS$ is such that

$$iRBS(\theta) |01\rangle = \cos(\theta) |01\rangle - i \sin(\theta) |10\rangle, \quad (D3)$$

$$iRBS(\theta) |10\rangle = \cos(\theta) |10\rangle - i \sin(\theta) |01\rangle. \quad (D4)$$

while acting as the identity on $|00\rangle$ and $|11\rangle$.

Using combinations of RBS gates with appropriately defined angles, one can load bit strings into an unary encoded quantum state. Unary data loaders are quantum circuits used to construct states of the form

$$|x\rangle = \frac{1}{\|x\|} \sum_{1 \leq j \leq d} x_j |e_j\rangle \quad (D5)$$

for a given d -dimensional vector $\vec{x} = (x_1, \dots, x_d)$, where $|e_j\rangle$ is the unary representation of the number j , i.e. $e_j = 0^{j-1}10^{d-j}$. They are examples of amplitude encoding routines, as they encode classical data in the amplitudes of a quantum state.

The state in Equation D5 can for example be constructed as follows. Start with the all-0-state $|0\dots 0\rangle$ and flip its first qubit. Then, define a set of angles for RBS gates so that when those gates are applied to a qubit q_n and its neighbor q_{n+1} successively, one obtains the target state. Writing $\theta_0 = \arccos(x_1)$, $\theta_1 = \arccos(x_2/\sin(\theta_0))$, $\theta_2 = \arccos(x_3/(\sin(\theta_0)\sin(\theta_1)))$, \dots , and applying $RBS(\theta_n)$ to the pair of qubits (q_n, q_{n+1}) , one can construct the target state in Equation D5. This is the diagonal unary data loader, as represented by the circuit in Figure 11 for an 8-point dataset.

This approach to the encoding of vectors can be extended to matrices. A n -by- m matrix $A = [a_{i,j}]_{i,j}$ can be encoded in amplitudes by the quantum state

$$|A\rangle = \frac{1}{\|A\|} \sum_{i=1}^n \sum_{j=1}^m a_{i,j} |e_j\rangle |e_i\rangle. \quad (D6)$$

The use of RBS gates for unary data loading has found applications to Orthogonal Neural Networks [20], Nearest Centroid Classification [18], and solving Partial Differential Equations such as Navier-Stokes, using Quantum Fourier Networks [17].

RBS gates can also be used to implement the inner product of two vectors x and y , by loading the vector y and then unloading (i.e. executing the reversed data loading circuit) the vector x . This unary inner product routine is a key element of the implementation of low-depth amplitude estimation [15], which finds applications in quantum Monte Carlo simulations [24], leading notably to an unary quantum algorithm for option pricing [25].

2. RBS gates are partially bias-preserving

While RBS gates have interesting properties with respect to the unary encoding, they are not bias-preserving in the strict sense of the term. Fortunately, RBS gates are partially bias-preserving.

Theorem D.2. *RBS gates $RBS(\theta)$ are \mathcal{S}_1 -bias-preserving gates, where \mathcal{S}_1 is the subspace spanned by all 2-qubit quantum states of Hamming weight 1 (that is, unary quantum states spanned by $|01\rangle$ and $|10\rangle$).*

Proof. First, observe that any state in \mathcal{S}_1 is a linear combination of unary quantum states and that

$$RBS(\alpha |01\rangle + \beta |10\rangle) = \alpha' |01\rangle + \beta' |10\rangle, \quad (D7)$$

for complex numbers $\alpha, \alpha', \beta, \beta'$ satisfying:

$$\begin{cases} \alpha' = \alpha \cos(\theta) + \beta \sin(\theta) \\ \beta' = \beta \cos(\theta) - \alpha \sin(\theta). \end{cases}$$

Consider an arbitrary state $|\phi\rangle = \alpha |01\rangle + \beta |10\rangle \in \mathcal{S}_1$. Then $RBS(\theta) |\phi\rangle$. Moreover, for every state $|\phi\rangle \in \mathcal{S}_1$, it holds that

$$Z_1 Z_2 |\phi\rangle = -|\phi\rangle, \quad (D8)$$

$$Z_1 |\phi\rangle = -Z_2 |\phi\rangle. \quad (D9)$$

From Equation D1 and D2, the action of the RBS gate on the subspace \mathcal{S}_1 can be described as

$$RBS(\theta) |\phi\rangle = \cos(\theta) |\phi\rangle + \sin(\theta) Z_1 X_1 X_2 |\phi\rangle, \quad (D10)$$

and therefore

$$\begin{aligned} RBS(\theta) Z_1 |\phi\rangle &= \cos(\theta) Z_1 |\phi\rangle + \sin(\theta) X_1 X_2 |\phi\rangle \\ &= Z_1 (\cos(\theta) |\phi\rangle + \sin(\theta) Z_1 X_1 X_2 |\phi\rangle) \\ &= Z_1 RBS(\theta) |\phi\rangle. \end{aligned} \quad (D11)$$

Now, consider an arbitrary diagonal unitary D defined by

$$D = Z_1(\mu_1) Z_2(\mu_2) Z_{1,2}(\mu_{1,2}) \quad (D12)$$

where

$$Z_j(\mu_j) = \cos\left(\frac{\mu_j}{2}\right) |\phi\rangle - i \sin\left(\frac{\mu_j}{2}\right) Z_j |\phi\rangle, \quad (\text{D13})$$

$$ZZ_{1,2}(\mu_j) = \cos\left(\frac{\mu_{1,2}}{2}\right) |\phi\rangle - i \sin\left(\frac{\mu_{1,2}}{2}\right) Z_1 Z_2 |\phi\rangle. \quad (\text{D14})$$

Observing that

$$RBS(\theta)ZZ_{1,2}(\mu) |\phi\rangle = ZZ_{1,2}(\mu)RBS(\theta) |\phi\rangle, \quad (\text{D15})$$

$$\text{and } RBS(\theta)Z_j(\mu) |\phi\rangle = Z_j(\mu)RBS(\theta) |\phi\rangle, \quad (\text{D16})$$

it follows that $RBS(\theta)D |\phi\rangle = D \cdot RBS(\theta) |\phi\rangle$, and therefore the RBS gate is \mathcal{S}_1 -bias-preserving. \square

This property holds not only for $(i)RBS(\theta)$, but for other parity-preserving gates such as $A(\theta, \phi)$ (see e.g. [4, 13, 14]), $Givens(\theta)$ (see e.g. [2, 21]), $XY(\theta)$ (see e.g. [1]).

Appendix E: Detailed calculations of performance analysis of Block-PEC on bias-preserving gates

In this section, we calculate the Block-PEC sampling cost of the circuits $U_{(a)} = CNOT_{1,2}U_2$, $U_{(b)} = CNOT_{1,2}U_{1,2}$, $U_{(c)} = CNOT_{i,j}U_{j,k}$ ($i \neq k$), directly from their quasi-probabilistic distribution, assuming $p > 0$.

We write $\alpha_0 = \frac{1-p}{1-2p}$ and $\alpha_1 = -\frac{p}{1-2p}$, so that

$$U_2 = \alpha_0 I_2 \circ U_2 + \alpha_1 Z_2 \circ U_2 \quad (\text{E1})$$

$$U_{1,2} = \alpha_0^2 I_1 I_2 \circ U_{1,2} + \alpha_0 \alpha_1 (I_1 Z_2 + Z_1 I_2) \circ U_{1,2} + \alpha_1^2 Z_1 Z_2 \circ U_{1,2} \quad (\text{E2})$$

For the circuit $U_{(a)}$, $\gamma_{\text{blk}}(U_{(a)}) = \beta_0 - 3\beta_1$ with $\beta_0 = \alpha_0^3 + \alpha_1^3 = ((1-p)^3 - p^3)/(1-2p)^3 > 0$ (associated to the channel I_2) and $\beta_1 = \alpha_0 \alpha_1^2 + \alpha_1 \alpha_0^2 = (p^2(1-p) - p(1-p)^2)/(1-2p)^3 < 0$ (associated to Z_2), so that

$$\gamma_{\text{blk}}(U_{(a)}) = \frac{1+2p-2p^2}{(1-2p)^2} < \frac{1}{(1-2p)^3} = \gamma_{\text{std}}(U_{(a)}). \quad (\text{E3})$$

For the circuit $U_{(b)}$, $\gamma_{\text{blk}}(U_{(b)}) = \beta_0 - \beta_1 - 2\beta_2$, with $\beta_0 = \alpha_0^4 + \alpha_0 \alpha_1^3 + \alpha_1^2 \alpha_0^2 + \alpha_1^2 \alpha_0 \alpha_1 > 0$ (associated to the channel $I_1 I_2$), $\beta_1 = \alpha_0^3 \alpha_1 + \alpha_1 \alpha_0^3 + \alpha_0^2 \alpha_1^2 + \alpha_1^4 < 0$ (associated to the channel $Z_1 I_2$), $\beta_2 = 2\alpha_0^2 \alpha_1^2 + \alpha_0 \alpha_1^3 + \alpha_1 \alpha_0^3 < 0$ (associated to the channels $I_1 Z_2$ and $Z_1 Z_2$), so that

$$\gamma_{\text{blk}}(U_{(b)}) = \frac{1+2p-6p^2+4p^3}{(1-2p)^3} < \frac{1}{(1-2p)^4} = \gamma_{\text{std}}(U_{(b)}). \quad (\text{E4})$$

For the circuit $U_{(c)}$, $\gamma_{\text{blk}}(U_{(c)}) = \beta_0 - \beta_1 - 3(\beta_2 - \beta_3)$, with $\beta_0 = \alpha_0^4 + \alpha_1^3 \alpha_0 > 0$ (associated to the channel $I_1 I_2 I_3$), $\beta_1 = \alpha_0^3 \alpha_1 + \alpha_1^4 < 0$ (associated to the channel $I_1 I_2 Z_3$), $\beta_2 = \alpha_0^3 \alpha_1 + \alpha_1^2 \alpha_0^2 < 0$ (associated to the channels

$I_1 Z_2 I_3, Z_1 I_2 I_3, Z_1 Z_2 I_3$), $\beta_3 = \alpha_1^3 \alpha_0 + \alpha_1^2 \alpha_0^2 > 0$ (associated to the channels $I_1 Z_2 Z_3, Z_1 I_2 Z_3, Z_1 Z_2 Z_3$), so that

$$\gamma_{\text{blk}}(U_{(c)}) = \frac{1+2p-2p^2}{(1-2p)^3} < \frac{1}{(1-2p)^4} = \gamma_{\text{std}}(U_{(c)}). \quad (\text{E5})$$

Correlated dephasing noise The per-block approach to PEC still yields an improvement in terms of sampling cost when dealing with correlated dephasing noise. Indeed, consider the correlated dephasing noise channel over a n -qubit set A defined as:

$$C_p^{[A]} = (1-p)I^{\otimes n} + \sum_{I^{\otimes n} \neq B \subseteq A} \frac{1}{2^n - 1} p Z_{[B]}, \quad (\text{E6})$$

inverted as the noise channel

$$\left(C_p^{[A]}\right)^{-1} = \gamma_1 \left((1-p)I^{\otimes n} - \sum_{I^{\otimes n} \neq B \subseteq A} \frac{1}{2^n - 1} p Z_{[B]} \right), \quad (\text{E7})$$

with $\gamma_1 = \frac{1}{1-2p}$.

Writing $\alpha_0 = \gamma_1(1-p)$ and $\alpha_1 = -\frac{p}{3}\gamma_1$, we observe for the circuit $U_{(b)}$ that $\gamma_{\text{blk}}(U_{(b)}) = \beta_0 - 3\beta_1$ with $\beta_0 = \alpha_0^2 + 3\alpha_1^2 > 0$ (associated to the channel $I_1 I_2$) and $\beta_1 = 2\alpha_0 \alpha_1 + 2\alpha_1^2 < 0$ (associated to the channels $Z_1 I_2$ and $Z_1 Z_2$), so that

$$\gamma_{\text{blk}}(U_{(b)}) = \frac{3-4p^2}{3(1-2p)} < \frac{1}{(1-2p)^2} = \gamma_1^2 = \gamma_{\text{std}}(U_{(b)}) \quad (\text{E8})$$

for correlated dephasing noise.

A similar analysis can be done for the circuits $U_{(a)}$ and $U_{(c)}$.